The Astrophysical Journal, 581:912–924, 2002 December 20

CONTINUUM AND EMISSION-LINE STRENGTH RELATIONS FOR A LARGE ACTIVE GALACTIC NUCLEI SAMPLE

M. Dietrich and F. Hamann
Department of Astronomy, University of Florida, 211 Bryant Space Science Center, Gainesville, FL 32611-2055; dietrich@astro.ufl.edu

J. C. Shields and A. Constantin
Department of Physics and Astronomy, Ohio University, MS 251B, Clippinger Research Labs, Athens, OH 45701-2979

M. Vestergaard
Department of Astronomy, Ohio State University, 140 West 18th Avenue, Columbus, OH 43210-1173

F. Chaffee
W. M. Keck Observatory, 65-1120 Mamalahoa Highway, Kamuela, HI 96743

C. B. Foltz
Multiple Mirror Telescope Observatory, University of Arizona, Tucson, AZ 85721

and

V. T. Junkkarinen
Center for Astrophysics and Space Sciences, Code 0424, 9500 Gilman Drive, University of California at San Diego, La Jolla, CA 92093-0424
Received 2002 July 17; accepted 2002 August 26

ABSTRACT

We report on the analysis of a large sample of 744 type 1 active galactic nuclei, including quasars and Seyfert 1 galaxies across the redshift from $0 \lesssim z \lesssim 5$ and spanning nearly 6 orders of magnitude in continuum luminosity. We discuss correlations of continuum and emission-line properties in the rest-frame ultraviolet and optical spectral ranges. The well-established Baldwin effect is detected for almost all emission lines from O VI $\lambda1034$ to [O III] $\lambda5007$. Their equivalent widths are significantly anticorrelated with the continuum strength, while they are nearly independent of redshift. This is the well-known Baldwin effect. Its slope β, measured as $\log W_\lambda \propto \beta \log \lambda L_\lambda(1450\ \text{Å})$, shows a tendency to become steeper toward higher luminosity. The slope of the Baldwin effect also increases with the ionization energy needed to create the individual lines. In contrast to this general trend, the N V $\lambda1240$ equivalent width is nearly independent of continuum luminosity and remains nearly constant. The overall line behaviors are consistent with softer UV continuum shapes and perhaps increasing gas metallicity in more luminous active galactic nuclei.

Subject headings: galaxies: active — quasars: emission lines

1. INTRODUCTION

Broad emission lines (BELs) are a defining property of quasar spectra. Nearly 25 years ago Baldwin (1977) discovered an anticorrelation between the equivalent width in C IV $\lambda1549$, W_λ(C IV) and the continuum luminosity, L_λ(1450 Å), measured at 1450 Å in the quasar rest frame. This result was based on a sample of 20 quasars spanning $\sim$2 orders of magnitude in continuum luminosity in the redshift range $1.24 \lesssim z \lesssim 3.53$. It has become known as the "Baldwin effect" (hereafter BEff). The BEff was subsequently confirmed in C IV $\lambda1549$, as well as other BELs such as Lyα and O VI $\lambda1034$ (Véron-Cetty, Véron, & Tarenghi 1983; Baldwin, Wampler, & Gaskell 1989; Kinney, Rivolo, & Koratkar 1990; Osmer, Porter, & Green 1994; Zheng, Kriss, & Davidsen 1995; Green, Forster, & Kuraszkiewicz 2001; see Osmer & Shields 1999 for a recent review).

A major impetus for studying the BEff was that it might be useful for calibrating active galactic nuclei (AGNs) luminosities, e.g., based on W_λ(C IV). The AGNs could then be used as cosmological standard candles. But in the following years studies of bigger quasar samples revealed a large scatter in the anticorrelation of the continuum luminosity versus emission-line strength (Baldwin et al.1989; Zamorani et al. 1992). The BEff is nonetheless important as a diagnostic of AGN structure and, perhaps, metal abundances (Korista, Baldwin, & Ferland 1998). The relation between the continuum luminosity and the relative emission-line strengths and ratios can be used to study the evolution and physics of the quasar phenomenon (Baldwin 1999). In particular, this correlation can be used to test model predictions for the dependence of the shape of the continuum spectral energy distribution as a function of luminosity (Binette et al. 1989; Netzer, Laor, & Gondhalekar 1992; Zheng & Malkan 1993; Wandel 1999a, 1999b).

The most fundamental problem, however, is that the physical cause of the BEff remains unknown. It was suggested by Mushotzky & Ferland (1984) that the observed relation can be explained by an anticorrelation of the ionization parameter, U, and the continuum luminosity, with $U = Q(\mathrm{H})/4\pi r^2 c n_\mathrm{H}$, where Q(H) is the number of hydrogen ionizing photons emitted per second by the central continuum source, r is the distance between the continuum source and the emission-line region, and n_H is the hydrogen density in the line-emitting cloud. Assuming an additional relation of decreasing covering factor with increasing continuum strength, the observed BEff could be well described for C IV $\lambda1549$. However, this model does not naturally explain the

BEff in the full range of measured lines. It predicts, for example, a lack of a BEff for Lyα even though it is clearly detected (e.g., Kinney, Rivolo, & Koratkar 1990; Osmer et al. 1994; Laor et al. 1995; Green 1996).

Another important clue to the physical cause of the BEff is that the strength of the relationship (i.e., the slope of the W_λ–L_c anticorrelation) seems to depend on the ionization energy of the emission-line species (Zheng et al. 1995; Espey & Andreadis 1999). In particular, the equivalent widths of high-ionization lines such as O VI λ1034 decrease more dramatically with L_c than lines with moderate ionization energies such as C IV λ1549 or low-ionization energies such as Mg II λ2798 and Balmer emission lines. Our results in the present paper confirm this claim and improve upon the overall empirical characterization of the BEff correlations.

The BEff might result from a more fundamental correlation between the continuum luminosity, L_c, and the shape of the ionizing (EUV–soft X-ray) continuum (Binette et al. 1989; Zheng & Malkan 1993; Zheng et al. 1997; Korista et al. 1998). Netzer (1985, 1987) and Netzer, Laor, & Gondhalekar (1992) suggested accretion disk models to explain the observed continuum and emission-line correlations. Recently, Wandel (1999a,1999b) added to this the growth in black hole mass by accretion in the accretion disk model. His analysis predicts that the continuum luminosity increases toward higher black hole mass and that the shape of the ionizing continuum becomes softer. Hence, it is suggested that the BEff is driven by a softening of the ionizing continuum toward higher luminosities. This model is attractive because the UV–X-ray spectral softening has been well documented by observations (Tananbaum et al. 1986; Wilkes et al. 1994; Green et al. 1995) and because the spectral softening provides a natural explanation for steeper BEff slopes in higher ionization lines.

An additional possibility is that the BEff is driven, at least in part, by a trend for higher metallicities in more luminous AGNs. Korista, Baldwin, & Ferland (1998) presented theoretical results showing the dependence of the emission-line equivalent widths on both the continuum shape and the metallicity of the gas. Their proposal is based on evidence for higher metal abundances in more luminous quasars (Hamann & Ferland 1993, 1999; Dietrich et al. 1999; Dietrich & Wilhelm-Erkens 2000) and on the suggestion that more luminous quasars reside in more massive host galaxies, which will naturally be more metal rich (Cen & Ostriker 1999; Pettini 1999; Kauffmann & Haehnelt 2000; Granato et al. 2001; see Hamann & Ferland 1999 for a review).

Our combination of ground-based and satellite data also provides the opportunity to study evolutionary aspects of the line strengths in detail—e.g., by measuring the same rest-frame UV lines across a wide range of redshifts. One serious complication affecting previous work is that luminosity and redshift are often correlated in quasars samples, because the quasars are selected from magnitude-limited surveys. Most studies have supported the original claim by Baldwin (1977) that W_λ scales inversely with luminosity and that there is no significant trend with redshift z (e.g., Kinney, Rivolo, & Koratkar 1990; Osmer et al. 1994; Francis & Koratkar 1995; Wilkes et al. 1999). However, some recent work based on the Large Bright Quasar Survey (LBQS) claims that the relationship to redshift is even stronger than with luminosity (Forster et al. 2001; Green, Forster, & Kuraszkiewicz 2001).

The present paper is the first in a series in which we examine the emission-line properties in a large sample of 744 type 1 AGNs. The sample includes Seyfert 1 galaxies and both radio-loud and radio-quiet quasars spanning an unprecedented wide range in both redshift ($0 \lesssim z \lesssim 5$) and intrinsic luminosity ($\sim$6 orders of magnitude). The database and data processing will be described in detail in a future paper. A major concern regarding BEff studies is that selection effects in AGN samples, e.g., pertaining to emission-line strengths, might bias some measurements of the BEff. Our sample has the advantage of being drawn from a variety of surveys, with objects selected based on radio properties, grism spectroscopy, or broadband color criteria. Hence, no specific selection criteria were applied for the data. Another key advantage is that our sample includes a wide range of luminosities at various redshifts. We can therefore address the separate redshift and luminosity dependences in the emission-line data.

There are several interesting problems we wish to address. The most basic issue is to quantify the nature of empirical correlations with L_c and/or z. In an upcoming study we will further examine correlations with other AGN properties such as radio-loudness (Baldwin 1977; Sargent, Steidel, & Boksenberg 1989; Steidel & Sargent 1991; Francis & Koratkar 1995). We will also report on trends with L_c or z among various emission-line metallicity indicators. Here we present an initial analysis on the nature of the BEff. Our approach is to construct composite spectra for specific L_c and z intervals, thus providing high signal-to-noise spectra and allowing us to study trends in both weak and strong emission lines.

The AGN sample is described briefly in § 2 and the calculation and analysis of the composite spectra in §§ 3 and 4. The main results appear in several figures in § 5. We compare our results with prior studies and discuss them in the context of suggested models in § 6. Throughout this paper we use the cosmological parameters $H_0 = 65$ km s^{-1} Mpc^{-1}, $\Omega_M = 0.3$, and $\Omega_\Lambda = 0$ (Carroll, Press, & Turner 1992). Introducing $\Omega_\Lambda = 0.7$ (Netterfield et al. 2002) instead of $\Omega_\Lambda = 0.0$, the luminosities at the highest redshifts would be $\sim$10% smaller, while at low redshifts they would reach a maximum of $\sim$20% larger at redshift $z \simeq 1$.

2. THE QUASAR SAMPLE

We have compiled a large sample of rest-frame visible and ultraviolet spectra for 826 type 1 AGNs. A majority of the spectra were obtained by several groups for different studies over the last 20 yr using ground-based instruments as well as *International Ultraviolet Explorer* (*IUE*) and *Hubble Space Telescope* (*HST*) (Bahcall et al. 1993; Baldwin et al. 1989; Chaffee et al. 1991; Corbin & Boroson 1996; Kinney et al. 1991; Lanzetta, Turnshek, & Sandoval 1993; Laor et al. 1995; Sargent, Boksenberg, & Steidel 1988, 1989; Schneider, Schmidt, & Gunn 1991a, 1999b; Steidel 1990; Steidel & Sargent 1991; Steidel, unpublished; Storrie-Lombardi et al. 1996; Weymann et al. 1991, 1998; Wills et al. 1995; Zheng et al. 1997). In total, the sample contains 351 quasar spectra measured with *HST*. Furthermore, we observed a large number of the quasars in our sample at redshifts $z \gtrsim 3$ (Constantin et al. 2002; Dietrich et al. 1999; Dietrich & Wilhelm-Erkens 2000; Dietrich et al. 2002a, 2002b). For this study we exclude broad absorption-line quasars (BAL QSOs), although there are indications that their emission-line properties do not differ from non-BAL quasars (Weymann et al. 1991). We also excluded several quasar spectra with extremely poor signal-to-noise ratios. The sample we investigate consists of 744 type 1 AGNs.

Because this AGN sample was compiled from many independent projects, it encompasses a wide range of selection criteria. Most of the quasars, especially at high redshifts, were discovered by color selection techniques (e.g., Storrie-Lombardi et al. 1996) or found by objective prism surveys (e.g., Chaffee et al. 1991; Sargent et al. 1988, 1989; Schneider at al. 1991a, 1999b).

We used the radio flux densities given in Véron-Cetty & Véron (2001) to determine the radio loudness for the quasars. Following Kellermann et al. (1989), we calculated the parameter $R_L = \log(F_R/F_B)$ with F_R as the radio flux density at 5 GHz and F_B as the B-band flux, each in the rest frame. Our classifications of radio-loud quasars are consistent with classifications available in the literature (Wills et al. 1995; Bischof & Becker 1997; Wilkes et al. 1999; Stern et al. 2000). In total our sample contains 265 radio-loud quasars and 479 radio-quiet AGNs.

Kinney et al. (1990) and Pogge & Peterson (1992) pointed out that a significant fraction of the scatter in the BEff in Seyfert 1 galaxies is caused by variability. They found that observations obtained at multiple epochs for individual sources display a BEff-like correlation (the *intrinsic* BEff), but with a significantly steeper slope than the BEff observed for an ensemble of AGNs. The physical mechanisms which drive each effect might be different, i.e., the ensemble BEff might be due primarily to variations in black hole mass while the intrinsic BEff might be caused by changes of the accretion rate $\dot{M}$ (Green 1999). For eight of the 36 low-luminosity AGNs [$\log \lambda L_\lambda(1450\ \text{Å}) \leq 44$, for λL_λ in ergs s^{-1}], the spectra are means from intense monitoring campaigns (Crenshaw et al. 1996; Collier et al. 1998, 2001; Dietrich et al. 1993; Goad et al. 1999; Kaspi et al. 1996; Korista et al. 1995; Peterson et al. 1994; Reichert et al. 1994; Santos-Lleó et al. 2001; Stirpe et al. 1994; Wanders et al. 1997). At the high-luminosity end of the luminosity distribution, it has been shown that quasars vary on longer timescales and with smaller amplitudes (e.g., Kaspi et al. 2000). For these reasons, the scatter caused by intrinsic variability is not expected to strongly influence our analysis of the present large quasar sample, particularly when comparisons of composite spectra are employed.

We transformed each quasar spectrum to the rest-frame using a redshift measured from C IV $\lambda1549$. To determine the redshift we fitted a Gaussian profile to the upper part of the C IV $\lambda1549$ emission line having $I_\lambda \geq 50\%$ of the peak intensity. We corrected each AGN spectrum for Galactic extinction (Seaton 1979), based on the neutral hydrogen column density $N_{\rm H}$ expressed in units of 10^{20} cm^{-2}, assuming $E_{B-V} = N_{\rm H}/60$ (Dickey & Lockman 1990).

The redshift distribution of the quasar sample is presented in Figure 1 as a function of continuum luminosity, $\lambda L_\lambda(1450\ \text{Å})$. The quasars cover a redshift range of $0 \lesssim z \lesssim 5$ and nearly 6 orders of magnitude in luminosity. For most of the redshift range a reasonable coverage in luminosity is achieved, spanning at least 3 orders of magnitude for $z \gtrsim 1$. The radio-loud and radio-quiet quasars are displayed with different symbols in Figure 1. Their distributions across luminosity and redshift are very similar within out sample, although the fraction of radio-loud quasars increases for redshifts $z \lesssim 2$.

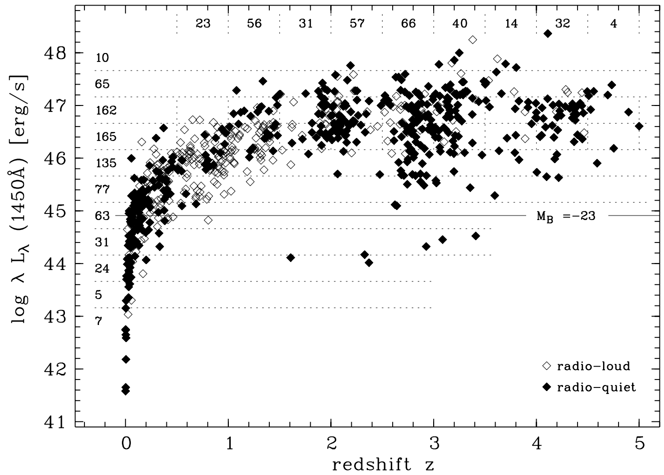

FIG. 1.—Redshift distribution of the quasar sample as a function of intrinsic luminosity at $\lambda = 1450$ Å. The open symbols represent radio-loud quasars and the filled symbols radio-quiet quasars. The dashed horizontal lines indicate the luminosity ranges that were used to calculate composite spectra. At the left-hand side of the figure is the number of the individual spectra contributing to each composite spectrum. For the luminosity range $46.1 \leq \log \lambda L_\lambda(1450) \leq 47.1$, composite spectra were calculated for the redshift intervals marked by the vertical dashed lines. The number of spectra contained in each redshift bin is given at the top of the figure.

3. COMPOSITE SPECTRA

A common approach to study the BEff is to measure the emission-line properties of individual quasars. However, the results are often limited especially for the weaker emission lines by the low signal-to-noise ratio of individual spectra. There can also be significant problems introduced by including upper limits on weak lines in individual spectra. To avoid those problems, we computed composite spectra in different intervals of redshift and luminosity. The analysis of these spectra has the advantage of more clearly representing the average properties of the sample used to calculate each composite. Figure 1 indicates the ranges in luminosity and redshift used to compute the composites. Except for the low- and high-luminosity ends of our sample, each composite spectrum is based on more than 20 individual quasar spectra. The scatter introduced by different individual spectra is taken into account by calculating a rms (standard deviation) spectrum for each composite and using that to estimate the uncertainties in the measured equivalent widths (§ 4).

Before combining the individual quasar spectra, we normalized the flux densities to unity in a 20 Å wide continuum range centered at $\lambda = 1450$ Å by multiplying each spectrum with a suitable factor. We used these normalized quasar spectra to calculate the mean and rms spectrum for each composite and the number of spectra contributing in each wavelength bin.

To avoid the influence of strong narrow absorption lines, we developed a search routine to detect strong narrow absorption features and exclude them from the calculation of the composite spectrum. To search for strong absorption lines we applied the following method (a more detailed description will be given in a subsequent paper on the properties of the entire quasar sample; M. Dietrich & F. Hamann 2002, in preparation). First, a preliminary mean spectrum is calculated for the sample of spectra under study. We then divided each individual spectrum by this preliminary mean

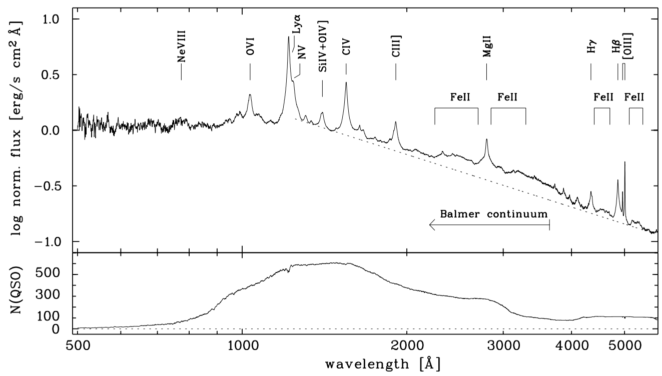

FIG. 2.—Composite spectrum of the quasar sample (*top*). The dashed line shows a power-law fit to the continuum (1200 Å $\leq \lambda \leq$ 5800 Å) yielding $\alpha = -0.43$ ($F_\nu \propto \nu^\alpha$). The bottom panel displays the number of quasars contributing to each wavelength element.

to derive a ratio spectrum. Each ratio spectrum is smoothed with a running boxcar function, which provides in addition to the mean also an rms value for each wavelength box. The resulting rms spectrum indicates the scatter in flux for each wavelength element in the immediate spectral region. A narrow absorption line will cause a sharp increase in the rms spectrum. The contaminated spectral regions of individual spectra, identified by these rms spikes, are excluded from the calculation of the final composite spectrum, and no interpolation has been applied. Multiple tests with different AGNs and different sample sizes show that this technique successfully removes strong narrow absorption lines from our composite spectra (see below) without affecting the emission lines. Significant effects of narrow absorption lines remain only in the Lyα forest ($\lambda \lesssim 1216$ Å) for composites that include quasars with redshift $z \gtrsim 1$.

The resulting composite quasar spectrum for the entire sample is shown in Figure 2. A single power-law fit to the continuum at $\lambda \geq 1200$ Å is also displayed; it has a slope of $\alpha = -0.43$ ($F_\nu \propto \nu^\alpha$). This spectral index is consistent with the slope reported for other composite spectra (Brotherton et al. 2001; Vanden Berk et al. 2001; Telfer et al. 2002). The bottom panel of Figure 2 shows the number of quasars contributing to each individual wavelength element. For every wavelength $800 \lesssim \lambda \lesssim 5600$ Å this composite quasar spectrum is based on at least $\sim$100 quasars.

4. EMISSION-LINE MEASUREMENTS

To measure the emission-line fluxes we analyzed each composite spectrum with spectral fitting software provided by MIDAS.[1] We employed a power-law continuum, an ultraviolet and optical Fe-emission template, a Balmer continuum emission template, and multiple Gaussian profiles for the broad emission lines in multicomponent fits using χ^2 minimization. For the ultraviolet wavelength range we used the Fe emission template that Vestergaard & Wilkes (2001) carefully derived from *HST* spectra of I Zw 1. The primary aim was to measure the broad and prominent Fe II emission near Mg II λ2798. However, we also used the UV template to correct for Fe II and Fe III emission blended with C III] λ1909 and other lines across the wavelength range 1400 Å $\lesssim \lambda \lesssim$ 1900 Å. For the optical wavelength region around Hβ and Hγ, we used the empirical Fe II emission template obtained from I Zw 1 (kindly provided by T. Boroson; Boroson & Green 1992). We adjusted the line widths in these Fe emission templates to match the measured widths of C IV λ1549, Mg II λ2798, or Hβ.

We calculated several bound-free Balmer continuum emission spectra for $T_e = 15000$ K, $n_e = 10^8$–10^{10} cm^{-3}, and $0.1 \leq \tau_\nu \leq 2$, following the formalism suggested by Grandi (1982). These Balmer continuum emission templates were supplemented for $\lambda > 3646$ Å with high-order Balmer emission lines with $10 \leq n \leq 50$, i.e., Hϑ and higher (Storey & Hummer 1995). The individual high-order Balmer lines were represented by Gaussian profiles and co-added.

The multicomponent fit of a Balmer continuum, two Fe emission templates, and a power-law continuum yields independent measurements of the ultraviolet and optical Fe-emission strengths. Furthermore, the spectral index, α, of the power-law continuum does not include contributions from Balmer continuum or from broad Fe emission. The uncertainties associated with the fit of Balmer continuum emission and Fe emission templates were estimated from the χ^2 distribution for each fit (see Dietrich et al. 2002a).

The emission-line fluxes were measured after subtracting the power-law continuum, Balmer continuum, and Fe emission spectra. The line fluxes were determined by multicomponent Gaussian fits. In general, we fitted the emission lines with a "broad" and a "narrow" Gaussian component. For C IV λ1549, however, it was necessary to introduce in addition a very broad component (which turned out to have typically FWHM $\simeq 10^4$ km s^{-1}). To determine the fluxes of Lyα and N V λ1240, which are severely blended, we used the components obtained from the C IV λ1549 profile as templates (preserving their widths and redshifts; see Fig. 2 in M. Dietrich & F. Hamann 2002, in preparation) for examples of fitted profiles. Note that most of the Lyα forest absorption on the blue side of the Lyα profile is corrected by the method we applied to calculated the composite spectra. The O VI λ1034 emission line is subject to severe corruption by Lyα forest absorption. However, in composite spectra it can be assumed that the same fraction of the O VI λ1034 emission-line flux and the adjacent continuum flux is absorbed by the Lyα forest. Hence, the equivalent width is not expected to be significantly altered by Lyα forest absorption. The O VI λ1034 emission line is also contaminated by Lyβ emission in the blue wing, whose relative strength shows a wide range, Lyβ/O VI $\lambda1034 = 0.30 \pm 0.21$ (Laor et al. 1995). Our fits to the O VI λ1034 emission-line profiles were achieved with a broad and narrow Gaussian profile, and no additional component due to Lyβ emission was necessary.

The C III] λ1909 emission-line complex was reconstructed with four Gaussian profiles, corresponding to Al III λ1857, Si III] λ1892, and broad and narrow Gaussian profiles for C III] λ1909. The correction for Fe emission allows a better measurement of Mg II λ2798, He II λ1640, N III] λ1750, and the C III] emission-line complex (Al III λ1857, Si III] λ1892, C III] λ1909). The measurement of the optical Fe II emission with an appropriate scaled template made it possible to measure the He II λ4686 emission line, which is otherwise severely blended with Fe II (37, 38) multiplets.

The cumulative errors in the emission-line flux measurements and W_λ were calculated as the square root of the sum of (1) the uncertainties in the χ^2 fitting and (2) the rms scat-

[1] Munich Image Data Analysis System, trademark of the European Southern Observatory.

ter that is introduced by both the noise and distribution of the individual spectra contributing to that particular composite spectrum, squared.

5. RESULTS AND ANALYSIS

5.1. *Trends with Redshift*

To search for a dependence of emission-line properties, particularly W_λ, on cosmic time (redshift), we selected a narrow luminosity range. The location of this luminosity range was also selected to achieve a comparable number of individual quasars contributing to each redshift bin in the z–$\lambda L_\lambda(1450\ \text{Å})$ plane. To cover a redshift range as large as possible for an almost constant luminosity, we selected a luminosity range of $46.16 \leq \log \lambda L_\lambda(1450\ \text{Å}) \leq 47.16$ [i.e., $43.0 \leq \log L_\lambda(1450\ \text{Å}) \leq 44.0$]. This range contains 323 quasars with $z \geq 0.5$ and an average luminosity of $\log \lambda L_\lambda(1450\ \text{Å}) = 46.67 \pm 0.12$. We computed composite spectra for redshift bins with $\Delta z = 0.5$ centered on redshift $z = 0.75,\ 1.25, \ldots, 3.75,\ 4.25$, and 4.75, respectively (Fig. 1). Figures 3*a* and 3*b* show the composite spectra for each redshift bin. These composite spectra are normalized by the power-law continuum that we derived from the multicomponent fits in § 4.

As a first impression, the relative line strengths in the normalized composite quasar spectra stay nearly constant with redshift z. However, some emission lines show a marginal trend for increasing equivalent width at the highest redshifts. To quantify this result, we measured the equivalent width of most emission lines in the ultraviolet wavelength range (λλ1000–3000) and of the broad ultraviolet Fe II emission feature (λλ2200–3090). The results for W_λ as a function of redshift are displayed in Figures 4*a* and 4*b*. In general, the equivalent widths of the lines remain constant within ∼30%. The stronger emission lines, however, such as Lyα, C IV λ1549, and C III] λ1909, show marginal trends for a relation of W_λ and redshift. The width W_λ stays nearly constant within less than ∼20% for redshifts less than $z \simeq 2$–3, but then for $z \gtrsim 3$ there are marginal indications for a slight increase of W_λ at constant luminosity. Close inspection of Figures 4*a* and 4*b* indicates that in particular the equivalent widths measured for the composites with $z \gtrsim 4$ are larger compared to lower redshifts. Most of the quasar spectra in our sample with $z \gtrsim 4$ were obtained by Constantin et al. (2002). They found evidence that in spite of strong contamination by Lyα-forest absorption, Lyα is stronger for quasars with $z > 4$ than in their low-z counterparts.

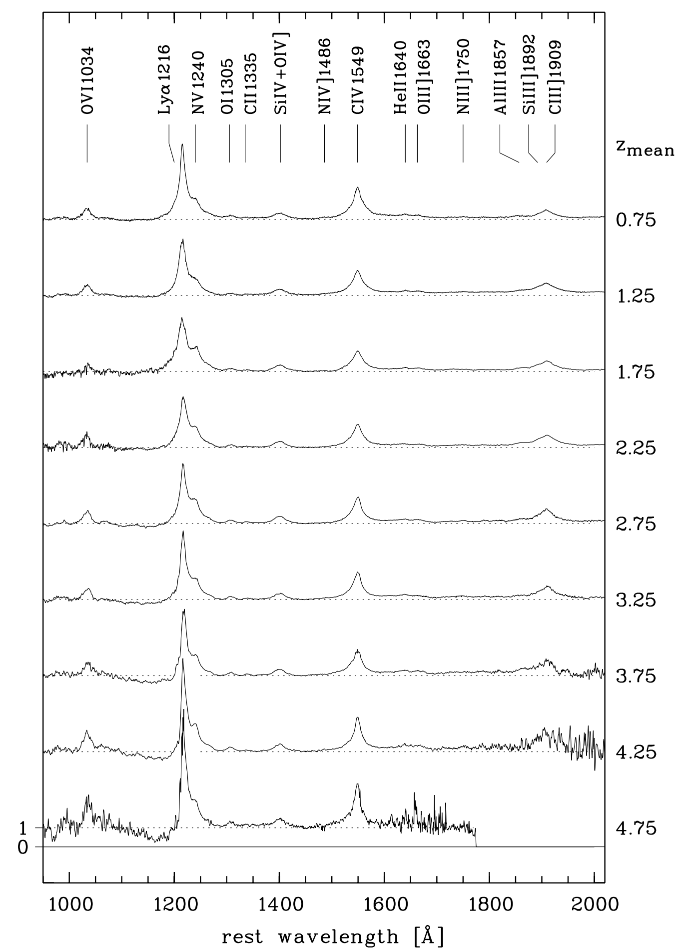

FIG. 3*a*

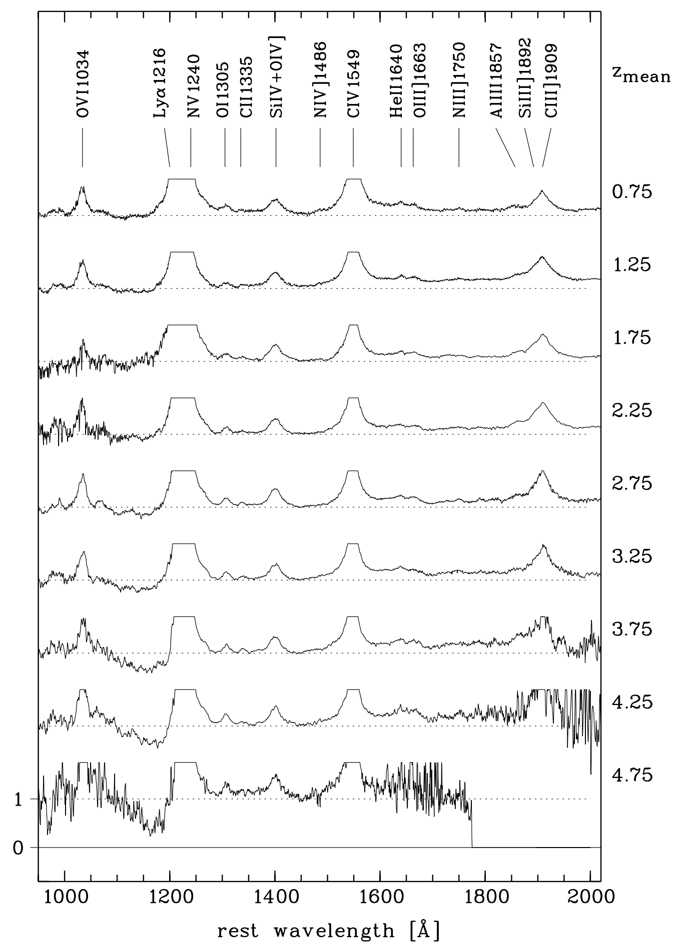

FIG. 3*b*

FIG. 3.—(*a*) Normalized composite spectra are shown for redshift bins of $\Delta z = 0.5$, starting at $z = 0.5$ (see Fig. 1) and nearly constant luminosity [$46.1 \leq \log \lambda L_\lambda(1450) \leq 47.1$]. The spectra were normalized with the corresponding power-law continuum fit. The horizontal dashed lines indicate the continuum level for the individual normalized composite spectra, which were vertically shifted for better display. The normalized continuum strength is shown for the spectrum at the bottom of the figure, and it applies for the other spectra, too. (*b*) Same as (*a*), but with an expanded vertical scale to display the dependence of the relative strength of weaker emission lines as a function of redshift. Strong emission lines with flat tops are truncated for easier display.

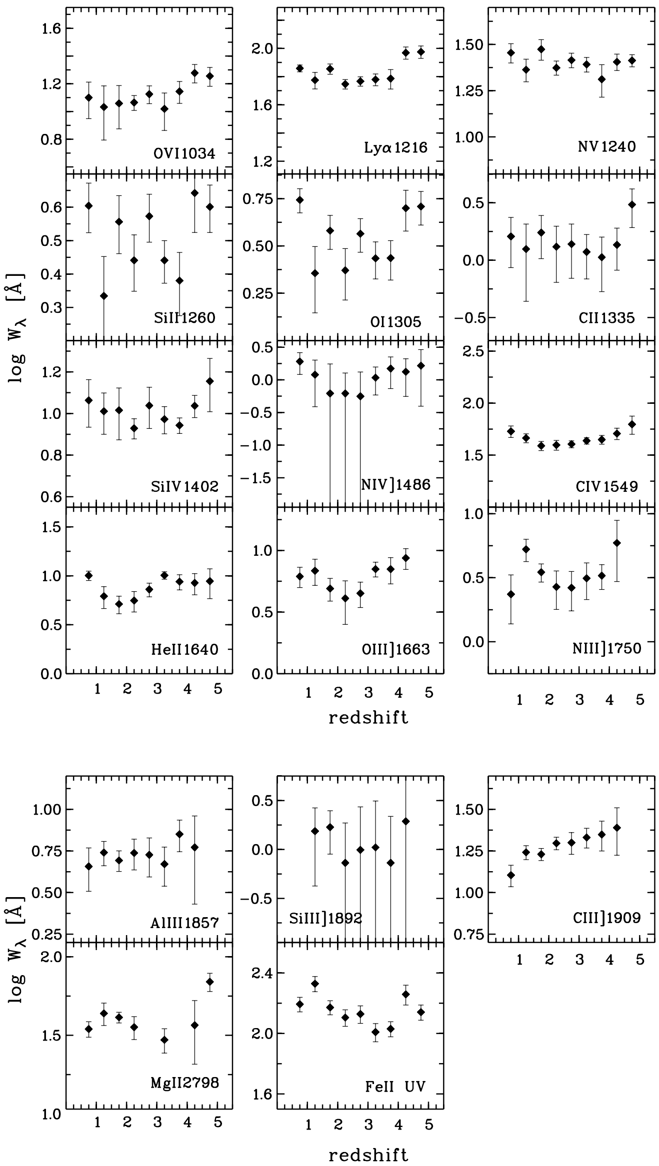

FIG. 4.—Line equivalent widths, W_λ, vs. redshift for nearly constant intrinsic continuum luminosity λL_λ(1450 Å).

5.2. *Trends with Luminosity*

Next we divided the quasar sample into 11 subsets with respect to the luminosity L_λ(1450 Å). Except for the lowest luminosity bin, each composite spectrum covers a range of $\Delta \log \lambda L_\lambda = 0.5$ in luminosity starting at $\log \lambda L_\lambda(1450\ \text{Å}) = 43.16$ ergs s^{-1} (Fig. 1). The two lowest luminosity composite spectra consist of less than 10 objects.

Figures 5*a* and 5*b* show the composite spectra ordered by luminosity for the ultraviolet wavelength range ($\lambda \lesssim 2000$ Å), while Figure 6 shows the longer wavelengths ($\lambda\lambda$2000–5600). Each composite spectrum is normalized by the power-law continuum fit we derived from the multicomponent analysis (§ 3). These normalized spectra show very obviously a strong relation between the equivalent width, W_λ, and the continuum luminosity represented by λL_λ(1450 Å), i.e., the BEff, for most of the emission lines. Figures 7*a* and 7*b* show the measured values of W_λ for each luminosity interval. The BEff can be seen easily in strong lines such as C IV λ1549, O VI λ1034, Lyα λ1216, C III] λ1909, and Mg II λ2798 (Figs. 5*a* and 6). Taking advantage of the high signal-to-noise ratio of the composite spectra, we also detected this relation for weaker emission lines such as He II λ1640. Furthermore, emission lines of the same ion but at different wavelengths (O III] λ1663, [O III] λ5007, He II λ1640, and He II λ4686) possess nearly identical slopes (Table 1). For the first time, we report on the BEff for N IV] λ1486, O III] λ1663, and N III] λ1750. In spite of the large scatter, the broad Fe emission features in the ultraviolet show some indications of a BEff, while within the errors, the optical Fe II emission lacks a BEff. In addition to the broad emission lines, we detect the BEff also for the prominent forbidden emission line [O III] λ5007 (Fig. 6), which is regarded as a typical narrow-line region (NLR) emission line. In contrast to the strong BEff in most of the emission lines visible in Figures 5*a*, 5*b*, and 6, the Balmer lines Hγ and Hβ show only weak indications of a BEff, which might be restricted to the line center of the line profiles. Close inspection of the N V λ1240 emission line (Figs. 5*a* and 8) also indicates that this line does not exhibit a BEff like other high-ionization lines. Lines having the same equivalent widths in each individual spectrum will cancel out in difference spectra (provided that their profiles are also the same), while lines whose equivalent widths are a function of luminosity will still be present in difference spectra. Note that N V λ1240 has on average cancelled out in the difference spectra as shown in Figure 8. Hence, the difference spectra near N V and the careful deblending of the Lyα–N V λ1240 emission-line complex both reveal that N V λ1240 remains nearly constant in W_λ over $\sim$6 orders of magnitude in continuum luminosity.

5.3. *Trends with Ionization Energy*

Zheng, Fang, & Binette (1992), Espey, Lanzetta, & Turnshek (1993), and Espey & Andreadis (1999) have suggested that there is a correlation between the ionization energy, $\chi_{\rm ion}$, of a specific emission line and the strength (slope) of the BEff. In contrast to Espey & Andreadis (1999), we use the ionization energy necessary to create the ion for collisionally excited lines such as C IV λ1549 and Mg II λ2798, and the ionization energy needed to ionize the ion for recombination lines such as Lyα and He II.

The BEff slope of the lines under study shows a relatively close linear correlation with $\chi_{\rm ion}$ (Figs. 7*a* and 7*b*). We determined the slope β, where $\log W_\lambda \propto \beta \log \lambda L_\lambda(1450\ \text{Å})$, of the BEff from a linear least-squares fit to $\log W_\lambda$ versus $\log \lambda L_\lambda(1450\ \text{Å})$. The fits were calculated taking into account the full uncertainties in $\log W_\lambda$. First, we calculated the slopes across the entire luminosity range, shown by the dotted line in Figures 7*a* and 7*b*. However, several of the emission lines indicate that the slope of the BEff is flatter at lower luminosities [$\log \lambda L_\lambda(1450\ \text{Å}) \lesssim 44$]. Therefore, we calculated additional linear fits for the luminosity range $\log \lambda L_\lambda(1450\ \text{Å}) \gtrsim 44$ (*dash-dotted lines*). It is interesting to note that the lines showing a change in the BEff slope have high-ionization energies with $\chi_{\rm ion} \gtrsim 25$–30 eV. The slopes of the $\log W_\lambda$ versus $\log \lambda L_\lambda(1450\ \text{Å})$ relations are listed in Table 1 and plotted against $\chi_{\rm ion}$ in Figure 9 for the entire range (*filled symbols*) and for $\log \lambda L_\lambda(1450\ \text{Å}) \gtrsim 44$ (*open symbols*). Notice that the slope of the BEff becomes steeper for increasing $\chi_{\rm ion}$. However, as has already been shown by earlier studies, N V λ1240 deviates significantly from this trend (Espey & Andreadis 1999). N V λ1240 stays constant or shows a slightly decreasing W_λ toward higher luminosity.

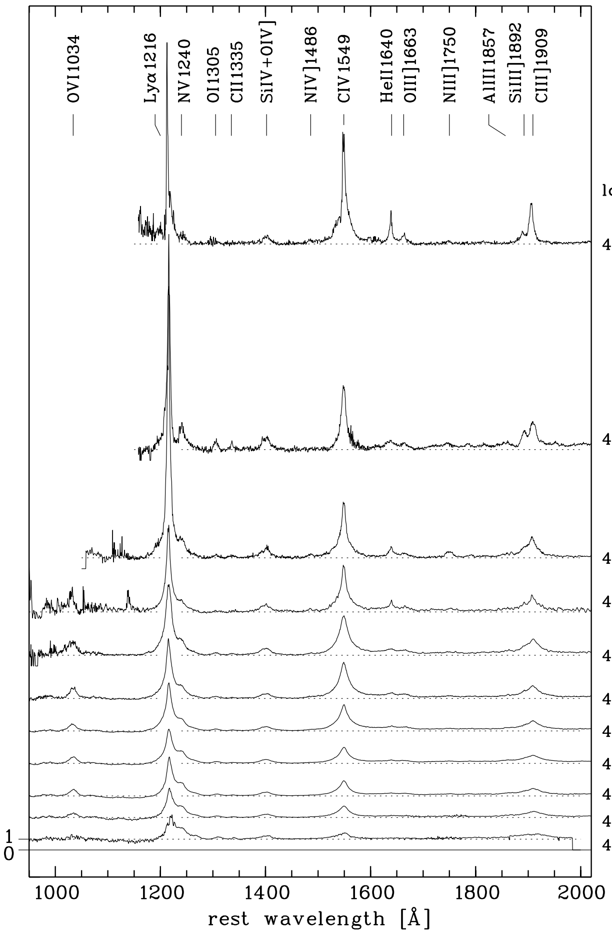

FIG. 5*a*

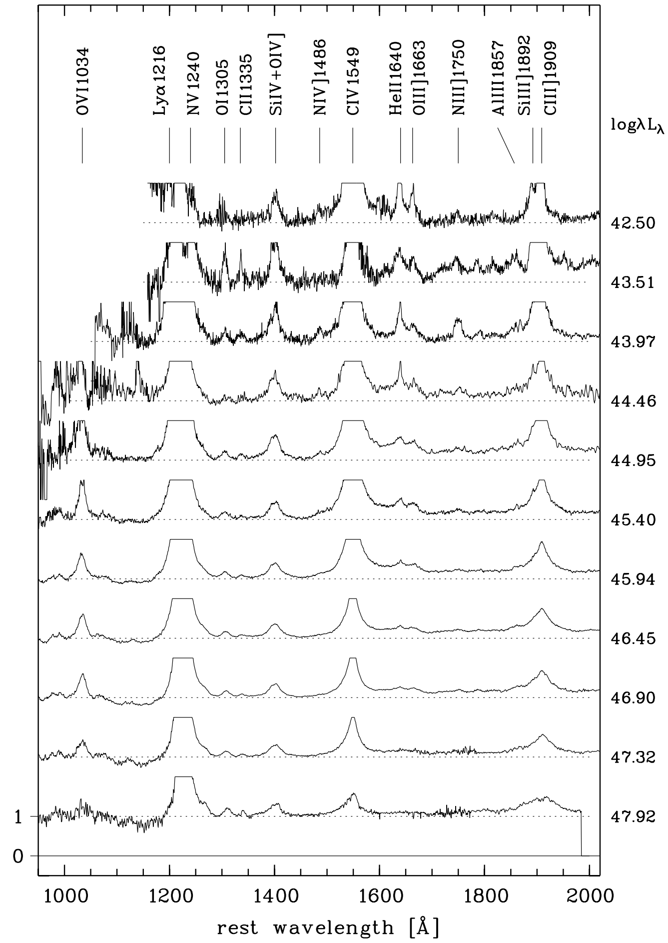

FIG. 5*b*

FIG. 5.—(*a*) Normalized composite spectra are shown for the luminosity bins [$\Delta \log \lambda L_\lambda$(1450 Å) = 0.5 dex)] as displayed in Fig. 1. The spectra were normalized with the corresponding power-law continuum fit. The horizontal dashed lines indicate the continuum level for the individual normalized composite spectra, which were vertically shifted for better display. The normalized continuum strength is shown for the spectrum at the bottom of the figure and it applies for the other spectra as well. (*b*) Same as (*a*), but with an expanded vertical scale to display the dependence of the relative strength of weaker emission lines as a function of luminosity. Strong emission lines with flat tops are truncated for easier display.

The slope β for O vi λ1034 is of particular interest for testing the hypothesis of a steeper BEff toward higher ionization energies since $\chi_{\rm ion}$(O^{+5}) is more than twice $\chi_{\rm ion}$(He^{+2}) and nearly 15 times $\chi_{\rm ion}$(Mg^{+}). Assuming a constant ratio of Lyβ /O vi $\lambda1034 = 0.30$ does not significantly change the slope of the BEff for O vi λ1034. However, β(O vi λ1034) would become steeper by nearly 25% if Lyβ follows the same BEff as Lyα and Lyβ /Ly$\alpha = 0.059 \pm 0.04$ (Laor et al. 1995).

To quantify the relationship of the BEff slopes β to $\chi_{\rm ion}$, we calculated linear least-squares fits to the points in Figure 9, excluding the outlying data point for N v λ1240. The resulting slope, η, is the same with ($\eta = -0.00154 \pm 0.00024$) or without ($\eta = -0.00150 \pm 0.00030$) the O vi λ1034 line included. This result indicates that O vi λ1034 does not dominate the β-$\chi_{\rm ion}$ relation.

6. DISCUSSION

6.1. *Comparisons with Other Studies*

In general, the slopes of the BEff derived here are consistent with prior investigations. However, the large range in both luminosity and redshift that distinguishes our quasar sample reveals correlations that were missed in some other studies. In particular, we can more clearly separate the trends with L and z, and our use of composite spectra across a wide luminosity range more accurately probes the BEff slopes, e.g., for weaker lines. In the following we provide some more detailed comparisons with earlier work.

The slopes we derived for Lyα λ1216, C i v λ1549, C iii] λ1909, and Mg ii λ2798 are in good agreement with prior studies (Kinney et al. 1990; Osmer et al. 1994; Laor et al. 1995; Green 1996; Turnshek 1997; Zamorani et al. 1992; Zheng et al. 1995; Wang, Lu, & Zhou 1998; Espey & Andreadis 1999). The steeper slopes for C iv λ1549 in Osmer et al. (1994), Laor et al. (1995), and Green (1996), $\beta = -0.23$ compared to $\beta = -0.14$ here, might be caused by the luminosity range of their quasar samples, $\lambda L_\lambda(1450\ \text{Å}) \gtrsim 10^{44}$ ergs s^{-1}. Using only the W_λ(C i v) measurements for $\lambda L_\lambda(1450\ \text{Å}) \gtrsim 10^{44}$ ergs s^{-1} in our sample, we calculate a slope of the BEff of $\beta = -0.20 \pm 0.03$ for C iv λ1549 (Table 1).

A lack of the BEff for C iv λ1549 and C iii] λ909 is reported by Wilkes et al. (1999). They conclude that this is caused by the narrow-line Seyfert 1 galaxies (NLSy1s) in their sample, which decrease the strength of the BEff; a significant BEff is found for both C iv and C iii] if the NLSy1s

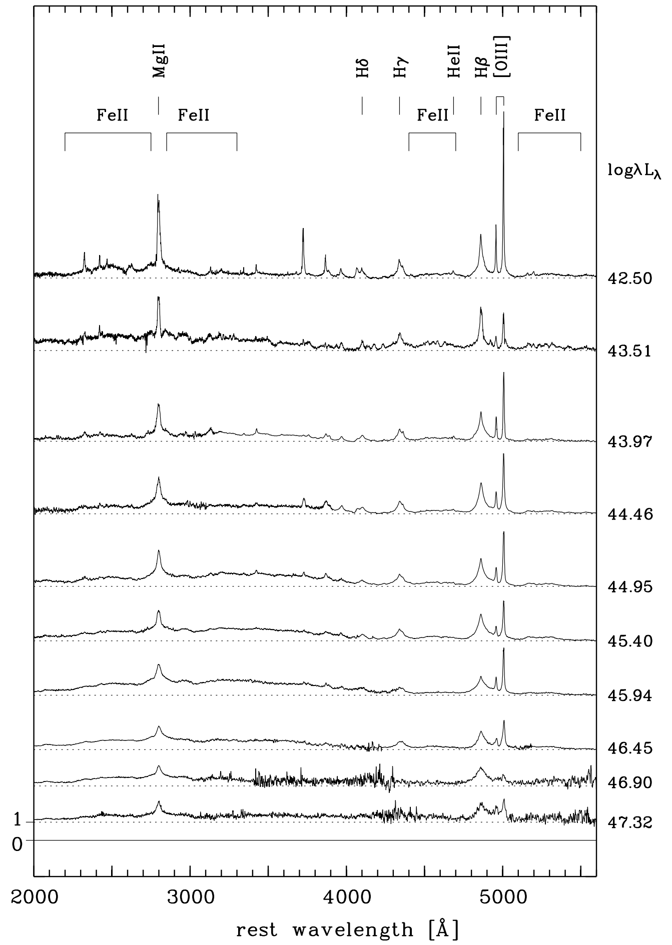

Fig. 6.—Same as Fig. 5, but the normalized composite spectra are shown at larger wavelengths.

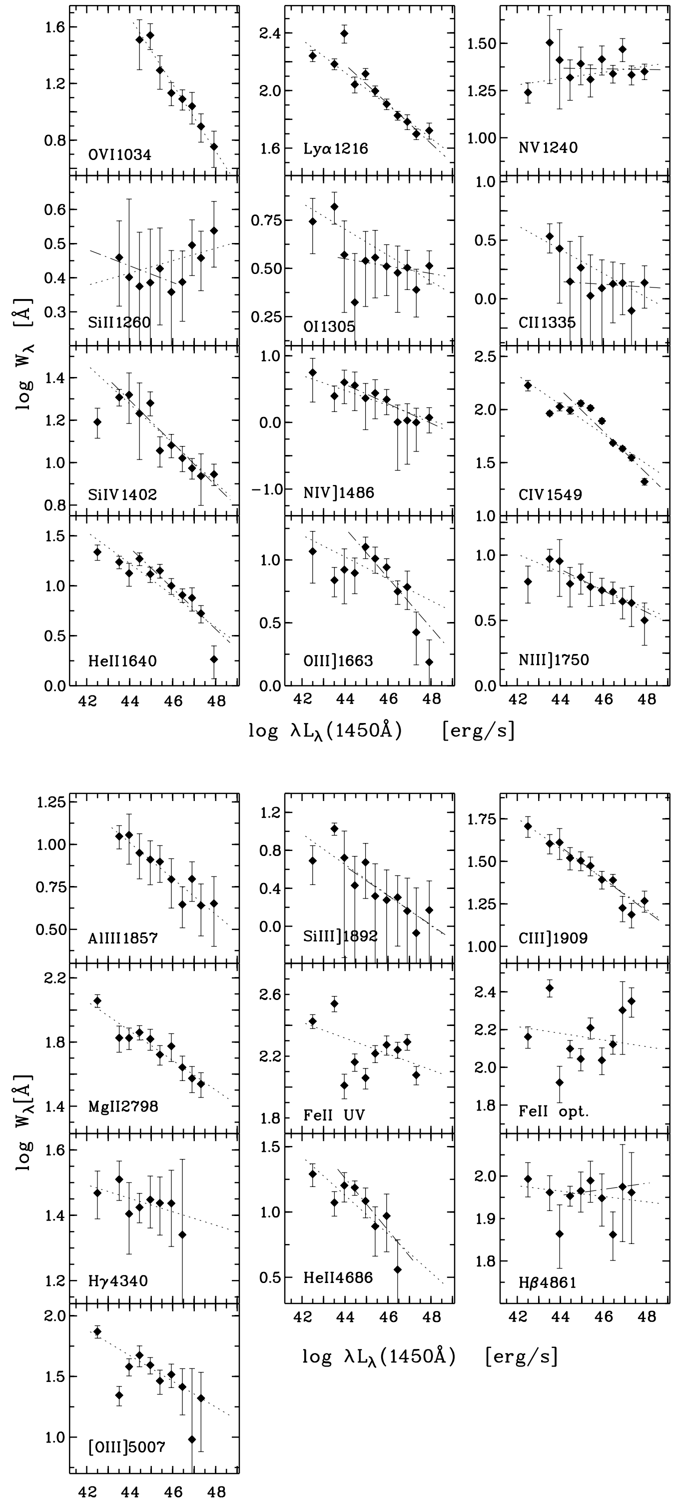

Fig. 7.—Line equivalent widths, W_λ, as a function of increasing continuum luminosity $\lambda L_\lambda(1450\ \text{Å})$. We calculated linear fits to $W_\lambda(L)$ for the entire luminosity range (*dashed line*), as well as a luminosities $\log \lambda L_\lambda(1450\ \text{Å}) \geq 44$ (*dash-dotted line*).

galaxies in their sample are omitted. We note that these NLSy1s are also low-luminosity AGNs. As can be seen in Figures 5*a* and 5*b*, the Baldwin relation is significantly flatter for low luminosities than at higher luminosities. Any AGN sample favoring a narrow luminosity range can dilute or bias the derived BEff. Similarly, the steeper BEff slopes reported by Laor et al. (1995) for O i λ1305, C ii λ1335, Si iv λ1402, and He ii λ1640 can be attributed to their smaller luminosity range [$\lambda L_\lambda(1350\ \text{Å}) \simeq 10^{45}$–$10^{48}$ ergs s^{-1}].

The slope for the BEff for the high-ionization emission line O vi λ1034 ($\chi_{\rm ion} \simeq 114$ eV) is also consistent with prior investigations. The reported slope β(O vi λ1034) varies between -0.30 ± 0.04 (Zheng et al. 1995; Turnshek 1997) and -0.15 ± 0.08 (Laor et al. 1995), with most recent studies favoring a less steep anticorrelation (-0.18 ± 0.03; Espey & Andreadis 1999). Wilkes et al. (1999) found only a marginal anticorrelation of W_λ(O vi λ1034) and continuum luminosity. However, they noted that this result is based on just 10 objects. Green (1996) and Green et al. (2001) did not detect a significant BEff for O vi λ1034 in their analysis of the LBQS data set, taking all quasar spectra into account, i.e., including upper limit measurements as well. However, using only those spectra with detected O vi λ1034, the BEff is clearly present. A possible reason for the missing BEff for O vi λ1034 in their study might be the very narrow luminosity range [$46.2 \lesssim \log \lambda\, L_\lambda(2500\ \text{Å}) \lesssim 47.0$] covered by LBQS quasars at these wavelengths. A comparison of our Figure 7*a* with Figure 2 in Green et al. (2001) shows that we measure the same range of O vi λ1034 equivalent widths for this luminosity, $\log W_\lambda(\text{O vi}\ \lambda1034) \simeq 1.1$. Hence, we conclude that the nondetection of the BEff for this high-ionization line in Green et al. (2001) is predominantly caused by their very small luminosity range.

TABLE 1

SLOPE β OF THE BALDWIN EFFECT FOR THE INDIVIDUAL EMISSION LINES

Line	χ_{ion} (eV)	β Entire λL_λ(1450 Å) Range	β $\log \lambda L_\lambda$(1450 Å) $\gtrsim$ 44	β Korista et al. (1998)
O VI λ1034	113.9	-0.24 ± 0.04	-0.24 ± 0.04	-0.22
N V λ1240	77.7	$+0.01 \pm 0.01$	-0.00 ± 0.02	-0.05
He II λ1640	54.4	-0.16 ± 0.03	-0.20 ± 0.04	-0.17
He II λ4686	54.4	-0.15 ± 0.04	-0.20 ± 0.09	...
C IV λ1549	47.9	-0.14 ± 0.02	-0.20 ± 0.03	-0.20
N IV] λ1486	47.4	-0.11 ± 0.04	-0.14 ± 0.08	-0.01
O III] λ1663	35.1	-0.09 ± 0.03	-0.20 ± 0.05	-0.12
[O III] λ5007	35.1	-0.10 ± 0.02	...	...
Si IV λ1402	33.5	-0.09 ± 0.01	-0.10 ± 0.02	-0.13
N III] λ1750	29.6	-0.07 ± 0.03	-0.08 ± 0.04	$+0.09$
Al III λ1857	28.4	-0.11 ± 0.03	-0.11 ± 0.03	-0.04
C III] λ1909	24.4	-0.09 ± 0.01	-0.09 ± 0.02	-0.08
Si III] λ1892	16.3	-0.16 ± 0.03	-0.16 ± 0.12	-0.06
Lyα λ1216	13.6	-0.11 ± 0.01	-0.14 ± 0.02	-0.10
Hγ λ4340	13.6	-0.02 ± 0.03	-0.02 ± 0.03	...
Hβ λ4861	13.6	-0.01 ± 0.01	$+0.01 \pm 0.03$	...
C II λ1335	11.3	-0.10 ± 0.04	-0.01 ± 0.09	$+0.00$
Si II λ1260	8.2	$+0.02 \pm 0.03$	-0.01 ± 0.09	...
Fe II UV	7.9	-0.05 ± 0.03	...	...
Fe II optical	7.9	-0.02 ± 0.03	...	...
Mg II λ2798	7.6	-0.09 ± 0.01	-0.09 ± 0.01	-0.09
O I λ1305	0.0	-0.07 ± 0.02	-0.02 ± 0.04	-0.05

NOTE.—A linear least-squares fit was calculated for the entire luminosity range and for $\log \lambda L_\lambda(1450\ \text{Å}) \gtrsim 44$; $\log W_\lambda = a + \beta \log \lambda L_\lambda(1450\ \text{Å})$. In addition, for comparison theoretical predictions are given (Korista et al. 1998; K. T. Korista 2002, private communication).

In contrast to Wills et al. (1999), we detect a significant BEff for the prominent NLR emission line [O III] λ5007 (Fig. 7*b*). The slope β of the anticorrelation is nearly identical to the one that we derived for O III] λ1663 (Table 1, Fig. 9). Again, the lack of a BEff for [O III] λ5007 in Wills et al. (1999) might be caused by the covered luminosity range of less than 2 orders of magnitude.

In agreement with prior investigations, we found no significant BEff for N V λ1240 (Osmer et al. 1994; Laor et al. 1995; Turnshek 1997; Espey & Andreadis 1999). Instead of a decreasing equivalent width for increasing continuum strength, W_λ(N V λ1240) stays nearly constant, even though it has a high value of $\chi_{ion} = 78$ eV.

6.2. *Comparison with Model Predictions*

Although much observational and theoretical effort has been spent to decipher the process that causes the BEff, the mechanism is still unclear. Several models have been suggested which emphasize different aspects, i.e., contributions from optically thin clouds and luminosity-dependent ionization parameter, covering factor, ionizing continuum shape, and chemical composition of the gas.

6.2.1. *Luminosity-dependent Ionization and Covering Factor*

The dependence of the strength of the BEff on the ionization energy indicates that a decreasing covering factor toward higher luminosities is not sufficient to explain the observed BEff for each emission line. To explain the observed BEff for C IV λ1549, Mushotzky & Ferland (1984) presented model calculations suggesting that the BEff is caused by a decrease of the ionization parameter, U, as well as the covering factor toward higher luminosities. Although this model predicts a weaker BEff for lower luminosity AGNs, it also predicts that Lyα will lack a BEff or show only a weak BEff. A luminosity dependence of the covering factor might be indicated independently by measurements of X-ray absorption (e.g., Lawrence & Elvis 1982).

A variant of this picture was outlined by Shields, Ferland, & Peterson (1995), who suggested that the luminosity dependence could be caused by a luminosity-dependent covering factor of optically thin clouds which would emit preferentially high-ionization lines. The presence of this component in the broad-line region (BLR) is suggested from several aspects of variability in Seyfert galaxies, as well as other arguments. While luminosity dependence of coverage by high-ionization clouds in the BLR is apparently still a viable scenario for understanding the BEff, this interpretation suffers from the lack of a strong physical basis for predicting this behavior; explanations are ad hoc or phenomenological at best.

6.2.2. *Luminosity-dependent Spectral Energy Distribution*

Several models have been advanced that focused primarily on the spectral energy distribution (SED) of the ionizing continuum and its consequences. This approach was motivated by increasing evidence that the SED of the continuum becomes softer for more luminous AGNs (e.g., Malkan & Sargent 1982; Binette et al. 1989; Schulz 1992; Netzer et al. 1992; Zheng et al. 1992; Zheng & Malkan 1993; Green 1996, 1998; Wang et al. 1998).

Empirical models have been suggested which combine a power-law continuum and a thermal UV bump. Detailed investigations of X-ray and ultraviolet continuum observations, i.e., the overall ionizing continuum shape, yield indications that the SED becomes softer for increasing

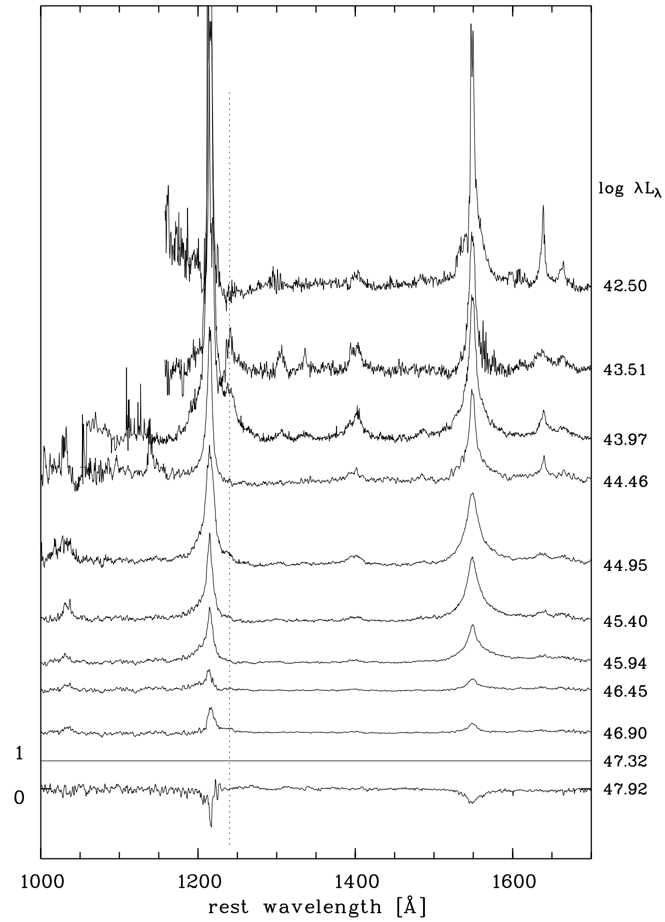

FIG. 8.—Difference spectra with respect to the composite spectrum $\log \lambda L_\lambda(1450\ \text{Å}) = 47.32$ are displayed to illustrate that W_λ(N v λ1240) is nearly constant, regardless of how W_λ(N v) is measured, while the other emission lines display a prominent BEff. The dotted line indicates the location of N v λ1240.

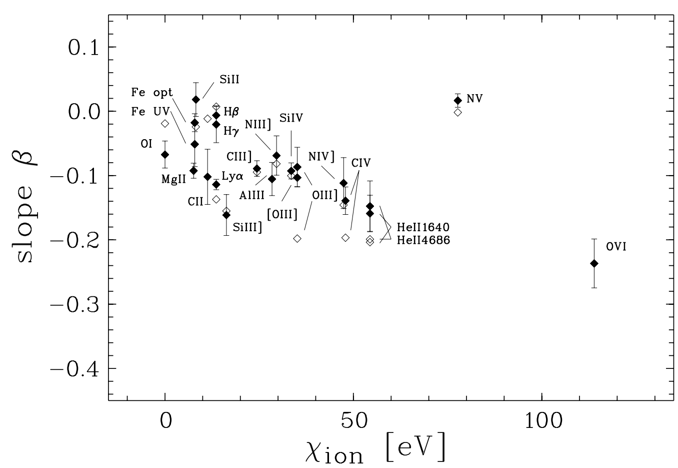

FIG. 9.—Slope of the BEff as displayed in Figs. 7*a* and 7*b* as a function of the ionization energy $\chi_{\rm ion}$ needed to create the specific ions. Different lines of the same ion (He II λ1640, He II λ4686, O III] λ1663, and [O III] λ5007) show nearly identical slopes. The filled symbols represent the slopes based on the entire luminosity range, corresponding to the dashed lines in Fig. 7*a*. The slopes of the BEff for higher luminosities only [$\log \lambda L_\lambda(1450\ \text{Å}) \geq 44$] are plotted as open symbols.

luminosity. In particular, it has been shown that $\alpha_{\rm ox}$, the two-point power index that connects the ultraviolet at 2500 Å to the X-ray continuum at 2 keV increases significantly with luminosity (Tananbaum et al. 1986; Wilkes et al. 1994; Green et al. 1995). This softening can be understood by a shift of the thermal UV-bump toward longer wavelengths in more luminous quasars, i.e., $L_{\rm uv}$ increases more than $L_{\rm X}$ for increasing luminosity resulting in a greater $\alpha_{\rm ox}$ (see Binette et al. 1989; Zheng & Malkan 1993).

Early models of geometrically thin and optically thick accretion disks focused on the consequences of the disk inclination and the location of gas relative to the disk (Netzer 1985, 1987). Although these models can not explain the BEff for several orders of magnitude in luminosity, they provide an explanation for scatter in the L_c-W_λ relation at a given luminosity. The SED of the accretion disk continuum depends on the luminosity, which is in turn related to the mass of the black hole and the accretion rate. These dependencies were suggested as the primary mechanism to cause the BEff. Recently, Wandel (1999a, 1999b) presented an evolutionary scenario that connects the growth of the black hole mass, the accretion rate, and the continuum luminosity. As the mass of the black hole increases and consequently also the luminosity, the peak temperature of the UV bump decreases. This results in a shift of the peak of the thermal UV bump to longer wavelengths, i.e., the continuum becomes softer. Netzer et al. (1992) calculated the $\log W_\lambda({\rm Ly}\alpha)$ versus $\log L_\lambda(1216\ \text{Å})$ relation for a wide range of black hole masses, accretion rates, and inclination angles in geometrically thin accretion disk models. The spread of the calculated $W_\lambda({\rm Ly}\alpha)$ at a given luminosity is mainly caused by the different inclination angles of the accretion disk. Assuming that our composite spectra represent an average over a variety of disk inclinations, the BEff that we measured for Lyα is consistent with their model predictions.

The observed ionization dependence of the BEff provides strong evidence for a luminosity-dependent SED of the ionizing continuum and thus favors accretion disk models. However, the detailed models discussed by Wandel (1999b) show that the SEDs of accretion disks depend in a complex way on the mass of the black hole and the accretion scenario. In particular, the cutoff energy of the thermal UV-bump is expected to depend on the black hole mass. These models also predict that luminous quasars with massive black holes should show low cutoff energies, while Seyfert 1 galaxies with intermediate massive black holes should display high cutoff energies. The low-luminosity NLSy1 galaxies with low-mass black holes should also exhibit high cutoff energies. Different accretion scenarios would introduce additional scatter to this relation.

In summary, accretion disk models provide a reasonable explanation of the BEff, in particular for the ionization energy $\chi_{\rm ion}$ dependent strength. Although these models indicate that the luminosity-dependent SED is a major mechanism that drives the BEff, the large possible parameter space allows for additional effects. Evidence for effects in addition to variations of the spectral energy distribution is given by the failure to explain the lack of a BEff for another high-ionization emission line, N v λ1240.

6.2.3. *The Influence of Metallicity Variations*

Baldwin et al. (1995) and Korista et al. (1997, 1998) introduced the "locally optimally emitting cloud" (LOC) model, which assumes that the BLR cloud ensemble covers a wide range of internal densities and occurs over a wide range in distance from the central continuum source. Under these conditions the emitted spectrum is controlled by powerful selection effects and the typical observed quasar spectrum can be naturally produced (Korista et al. 1997, 1998).

Korista et al. (1998) computed for a wide range of different continuum slopes ($F_\nu \propto \nu^\alpha, -2 < \alpha < -1$), densities ($n_e = 10^8$–$10^{12}$ cm^{-3}), and metallicities (0.2–10 times solar) the resulting emission-line spectra. In recent years there has been growing evidence that the chemical composition of quasar gas can reach several times solar metallicity with a trend of higher metallicities in more luminous quasars (Hamann & Ferland 1993, 1999; Ferland et al. 1996, Dietrich et al. 1999; Dietrich & Wilhelm-Erkens 2000). The emission lines studied by Korista et al. (1998) follow the general trend for W_λ diminishing with softer continuum shapes. Assuming the softer continua are related to higher luminosities, this yields the BEff. However, in contrast to those emission lines, N v λ1240 lacks a BEff even though its high-ionization energy $\chi_{\rm ion} = 78$ eV suggests that the decrease of W_λ(N v) should be strong. Korista et al. (1998) introduced metallicity as an additional parameter to provide a possible explanation for the lack of a BEff in N v λ1240. They found in their calculations that the equivalent width of Lyα, C iv λ1549, or O vi λ1034 show only a weak dependence on the gas metallicity, but N v λ1240 strongly depends on it.

In particular, they assume that nitrogen scales like a secondary element, so that its abundance relative to the other metals increases linearly with the overall metallicity (e.g., N/O $\propto$ O/H; see Hamann et al. 2002). Korista et al. (1998) assume that the metallicity increases with increasing AGN luminosity (Hamann & Ferland 1999). With this abundance behavior, Korista et al. (1998) showed that the equivalent width of N v λ1240 is not expected to display a BEff. Therefore, the decreasing equivalent width that should occur in N v λ1240 as part of the normal BEff is approximately compensated by the increasing relative abundance of nitrogen. The net result is that N v λ1240 shows essentially no BEff.

Overall, the BEff slopes that we derived for the emission lines in our quasar sample are in good agreement with the predictions by Korista et al. (Table 1). The observed slopes of C iv λ1549 and He ii λ1640 are smaller than expected, while the slope in N iii] λ1750 is steeper. However, if only measurements with $\lambda L_\lambda(1450\ \text{Å}) \gtrsim 10^{44}$ ergs s^{-1} are taken into account, the observations yield a comparable steep anticorrelation as predicted by Korista et al. (1998). We will discuss these comparisons further in a forthcoming paper on the trends in metallicity in this data set (see also § 6.4 below).

6.3. *Ionization Dependence and Curvature of the Baldwin Effect*

A common prediction of models that involve a softer continuum SED toward higher luminosities is a steeper slope of the BEff for lines with increasing ionization energy $\chi_{\rm ion}$ (Zheng et al. 1992; Zheng & Malkan 1993; Korista et al. 1998; Wandel 1999a). Figures 7*a*, 7*b*, and 9 provide clear evidence for this prediction. High-ionization lines such as C iv λ1549, He ii λ1640, He ii λ4686, and especially O vi λ1034 are particularly valuable. These emission lines respond to photoionizing energies of $\sim$48, $\sim$54, and $\sim$114 eV, respectively. Hence, they can be used to probe the location of the cutoff energy of the thermal UV bump. The strong BEff in these high-ionization lines is expected if the ionizing continuum becomes softer with increasing continuum luminosity. In this case the relative number of ionizing photons with $h\nu \gtrsim 50$ eV decreases as the UV bump is moving toward longer wavelengths. While there is only a marginal trend for a slightly steeper BEff for He ii than for C iv, the higher ionization O vi λ1034 line displays a significantly stronger BEff (Fig. 9). The decrease of the relative number of ionizing photons with a softer continuum, caused by the shift of the UV bump to longer wavelengths, results in weaker high-ionization lines compared to lower ionization ones. The shift of the UV bump to longer wavelengths will affect emission lines at higher ionization energy first. In addition, the relative continuum strength beneath the emission lines will be enhanced, starting at short ultraviolet wavelengths. Both effects together result in smaller W_λ for higher luminosities.

In addition to the general trend of steeper BEff for higher $\chi_{\rm ion}$, the curvature or flattening of the BEff toward lower luminosities can be accommodated in the framework of some of the luminosity-dependent SED models (e.g., Netzer et al. 1992; Wandel 1999a). The flattening at low luminosities has led to suggestions that Seyfert 1 nuclei do not participate in the BEff but have instead equivalent widths independent of luminosity (e.g., Wampler et al. 1984). A close inspection of Figures 7*a* and 7*b* provides some evidence for the tendency of a flatter slope β of the BEff at low luminosities in comparison to higher luminosities, as can be seen for several emission lines (Si iv λ1402, N iv] λ1486, C iv λ1549, He ii λ1640, O iii] λ1663, N iii] λ1750, and He ii λ4686). The turnover appears to occur near $\lambda \log L_\lambda(1450\ \text{Å}) \simeq 44$, in quite good agreement with predictions (Wandel 1999a). Within this context it is interesting to note that the steepening of the BEff for $\log \lambda L_\lambda(1450\ \text{Å}) \simeq 44$ is observed for emission lines with $\chi_{\rm ion} \gtrsim 25$–30 eV.

6.4. *Individual Emission-Line Pairs*

For several elements we have measured more than one emission-line strength. The comparison of the strength of the BEff may provide information about the emission-line region and the mechanism which causes the observed anticorrelation of W_λ and continuum luminosity.

For hydrogen we have measured two Balmer emission lines (Hγ and Hβ) and Lyα. The slope of the BEff of Hγ and Hβ is very similar and within the uncertainties consistent with zero, i.e., no BEff for Balmer lines. The missing BEff for these lines provide some argument against a luminosity-dependent covering factor, at least for the gas component, which is the dominant contributor to these emission lines. While the equivalent width W_λ(Hβ) remains nearly constant, the flux ratio Lyα/Hβ decreases by a factor $\sim$1.5 from low to high luminosities ($\sim$8.5 to $\sim$5.5). The different behavior of the Balmer lines and Lyα might be also related to the complex physical processes of Lyα and Hβ emission (Netzer et al. 1995). The prominent BEff of Lyα and the lack of a BEff for Hβ may be caused in part by a relative stronger increase of the local continuum beneath Lyα compared to the optical wavelength range of Hβ. However, Lyα shows a significant BEff that fits well in the slope β-$\chi_{\rm ion}$ relation

(Figs. 7*a*, 9). Lyα might be blended with He II λ1216 and O V] λ1218 (Ferland et al. 1992; Shields et al. 1995). For standard BLR conditions the contribution of He II λ1216 and O V] λ1218 are negligible (less than $\sim$10%; K. Korista 2002, private communication). But for higher densities and higher ionization parameter U, particularly for optically thin conditions, these emission lines can be quite strong compared to Lyα (Shields et al. 1995). Because O V] λ1218 has an ionization energy of $\chi_{\rm ion} = 77.4$ eV, this emission line might show a strong BEff. If optically thin gas is a significant fraction of the BLR gas, it might be possible that the moderate BEff of Lyα might be caused at least in part by O V] λ1218. However, if O V] λ1218 is a significant contamination of Lyα it is expected from the results in Shields et al. (1995) that He II λ1640 and C IV λ1549 should be stronger than observed. In addition, variability behavior in some objects suggests that the optically thin gas may contribute most strongly to the line wings (e.g., Ferland, Korista, & Peterson 1990; Peterson et al. 1993), but the part of the emission lines that changes the most with luminosity has a narrow FWHM (e.g., Osmer et al. 1994). Although we cannot exclude that O V] λ1218 provides some contribution to Lyα, it does appear that Lyα itself shows a moderate BEff in contrast to the Balmer emission lines.

The two emission lines of He^+ that we measured, He II λ1640 and He II λ4686, show very similar slopes for the BEff. This behavior is expected for He II λ1640 and He II λ4686 as typical recombination lines. The similar slope of the BEff provides also some evidence that luminosity-dependent radiative transfer effects, collisional effects or dust effects cannot affect these emission lines.

Another line pair we measured is O III] λ1663 and [O III] λ5007. While the ionization energy necessary to create O^{+2} is $\chi_{\rm ion} = 35.1$ eV, the excitation energies of these lines differ by a factor of $\sim$3. If the ionizing continuum becomes softer for increasing luminosity, the temperature in the emission-line region should drop and hence O III] λ1663 should be more affected than [O III] λ5007. Therefore, we might expect O III] λ1663 to have a steeper BEff than [O III] λ5007. Observationally their BEffs are the same. However, the comparison of these two lines is very complicated because they differ in critical density by several orders of magnitudes ($n_e^{\rm crit} \simeq 7 \times 10^5$ cm^{-3} for [O III] λ5007 and $n_e^{\rm crit} \simeq 3 \times 10^{10}$ cm^{-3} for O III] λ1663). In particular, [O III] λ5007 forms in the narrow-line region (NLR), which might be heated and ionized additionally by shocks, and is, in any case, spatially distinct from the BLR. The different kinematics of the O III–emitting gas is also given by the significantly different profiles we used to measure the emission-line flux and equivalent width. The O III] λ1663 emission line was fitted with a broad and narrow Gaussian profile (with an average FWHM of 5140 ± 460 and 1865 ± 290 km s^{-1}, respectively). The two Gaussian components we used to fit [O III] λ5007 result in a profile different compared to O III] λ1663, with average FWHMs of 1490 ± 50 and 480 ± 25 km s^{-1}. The overall average FWHM of the fitted O III] λ1663 and [O III] λ5007 lines are 4130 ± 450 and 725 ± 100 km s^{-1}, respectively.

We have studied three emission lines of nitrogen. N V λ1240 lacks within the errors a BEff. In contrast, the intercombination lines N IV] λ1486 and N III] λ1750 exhibit a BEff that is consistent with the overall trend of β-$\chi_{\rm ion}$ (Fig. 9). It might be possible that additional effects influence the emission properties of these nitrogen intercombination lines at higher luminosities. We will discuss these issues in our forthcoming paper on elemental abundances.

7. CONCLUSION

e have investigated a large sample of 744 type 1 AGNs covering the redshift range from $0 \leq z \leq 5$ and nearly 6 orders of magnitude in continuum luminosity. To enhance the signal-to-noise ratio, minimize the influence of peculiarities of individual quasars, and investigate weak as well as strong emission lines, we computed composite spectra representing narrow intervals in redshift and luminosity. The emission-line fluxes were derived using multicomponent Gaussian fits after removing a power-law continuum fit, a Balmer continuum emission template, and a UV and optical iron emission template from the composite spectra. Our main results are the following:

1. In composite spectra spanning the full redshift range at nearly constant luminosity we detect no strong trend in the line W_λ with redshift,i.e., with cosmic time. However, there is a marginal tendency for the highest redshift quasars ($z \gtrsim 4$) to show slightly stronger emission lines than their counterparts at lower redshift.
2. In the composite spectra ranked by luminosity we find a significant BEff in nearly all emission lines in the ultraviolet to optical domain. The only exceptions are N V λ1240, Hβ, Hγ, and optical Fe II, which remain constant in W_λ within the uncertainties. The lack of a BEff for the high-ionization feature NV λ1240 suggests that the chemical composition of the gas is an additional parameter that can strongly influence the equivalent width of this and possibly other lines.
3. We detect a strong BEff for the prominent NLR emission line [O III] λ5007. The strength of the BEff for [O III] λ5007 is very similar to the BEff measured in O III] λ1663.
4. The slope β of the BEff, where $\log W_\lambda \propto \beta \log \lambda\, L_\lambda$, shows a significant correlation with the ionization energy, $\chi_{\rm ion}$, needed to produce the lines.
5. The slope of the BEff, β, tends to be steeper at higher luminosities, $\lambda L_\lambda(1450\ \text{Å}) \gtrsim 10^{44}$ ergs s^{-1}, compared to the lower luminosity regime.
6. The BEff, its steepening toward higher luminosities, and the correlation of the slope β with $\chi_{\rm ion}$ can all be well explained in the context of a luminosity-dependent spectral energy distribution of the ionizing continuum. Assuming that the SED can be described as a combination of a power-law continuum and a thermal UV bump, the ionizing continuum becomes softer for increasing luminosity as the UV bump is shifted to longer wavelengths. This behavior can be explained with accretion disk models, as suggested by Netzer et al. (1992) and Wandel (1999a, 1999b).

We are grateful to numerous colleagues for providing many of these spectra in digital form, in particular J. A. Baldwin, T. A. Boroson, M. R. Corbin, A. Laor, W. L. W. Sargent, D. P. Schneider, C. C. Steidel, R. J. Weymann, and W. Zheng. M. V. Gratefully acknowledges financial support from the Columbus Fellowship. We also thank Desika Narayanan for reducing the spectra obtained at Lick Observatory. M. D. and F. H. have benefited from support from NASA grant NAG 5-3234 and NSF grant AST 99-84040.

REFERENCES

Bahcall, J. N., et al. 1993, ApJS, 87, 1
Baldwin, J. A. 1977, ApJ, 214, 679
———. 1999, in ASP Conf. Ser. 162, Quasars and Cosmology, ed. G. Ferland & J. A. Baldwin (San Francisco: ASP), 475
Baldwin, J. A., Ferland, G. J., Korista, K., & Verner, D. 1995, ApJ, 455, L119
Baldwin, J. A., Wampler, E. J., & Gaskell, C. M. 1989, ApJ, 338, 630
Binette, L., Prieto, A., Szuszkiewicz, E., & Zheng, W. 1989, ApJ, 343, 135
Bischof, O. B., & Becker, R. H. 1997, AJ, 113, 2000
Boroson, T. A., & Green, R. F. 1992, ApJS, 80, 109
Brotherton, M. S., et al. 2001, ApJ, 546, 775
Carroll, S. M., Press, W. H., & Turner, E. L. 1992, ARA&A, 30, 499
Cen, R., & Ostriker, J. P. 1999, ApJ, 519, L109
Chaffee, F. H., Foltz, C. B., Hewett, P. C., Francis, P., Weymann, R. J., Morris, S. L., Anderson, S. F., & MacAlpine, G. M. 1991, AJ, 102, 461
Collier, S., et al. 1998, ApJ, 500, 162
———. 2001, ApJ, 561, 146
Constantin, A., Shields, J. C., Hamann, F., Foltz, C. B., & Chaffee, F. H. 2002, ApJ, 565, 50
Corbin, M. R., & Boroson, T. A. 1996, ApJS, 107, 69
Crenshaw, D. M., et al. 1996, ApJ, 470, 322
Dickey, J. M., & Lockman, F. J. 1990, ARA&A, 28, 215
Dietrich, M., Appenzeller, I., Vestergaard, M., & Wagner, S. 2002a, ApJ, 564, 581
Dietrich, M., Hamann, F., Appenzeller, I., Vestergaard, M., & Wagner, S. J. 2002b, in Lighthouses of the Universe, ed. M. Gilanof, R. Sunyaev, E. & Churazof (New York: Springer), 329
Dietrich, M., & Wilhelm-Erkens, U. 2000, A&A, 354, 17
Dietrich, M., et al. 1993, ApJ, 408, 416
———. 1999, A&A, 352, L1
Espey, B. R., & Andreadis, S. J. 1999, in ASP Conf. Ser. 162, Quasars and Cosmology, ed. G. Ferland & J. A. Baldwin (San Francisco: ASP), 351
Espey, B. R., Lanzetta, K. M., & Turnshek, D. A. 1993, BAAS, 25, 1448
Ferland, G. J., Baldwin, J. A., Korista, K. T., Hamman, F., Carswell, R. F., Phillips, M., Wilkes, B., & Williams, R. E. 1996, ApJ, 461, 683
Ferland, G. J., Korista, K. T., & Peterson, B. M. 1990, ApJ, 363, L21
Ferland, G. J., Peterson, B. M., Horne, K., Welsh, W. F., & Nahar, S. N. 1992, ApJ, 387, 95
Forster, K., Green, P. J., Aldroft, T., Vestergaard, M., Foltz, C. B., & Hewett, P. C. 2001, ApJS, 134, 35
Francis, P. J., & Koratkar, A. P. 1995, MNRAS, 274, 504
Goad, M., et al. 1999, ApJ, 524, 707
Granato, G. L., Silva, L., Monaco, P., Panuzzo, P., Salucci, P., De Zotti, G., & Danese, L. 2001, MNRAS, 324, 757
Grandi, S. A. 1982, ApJ, 255, 25
Green, P. J. 1996, ApJ, 467, 61
———. 1998, ApJ, 498, 170
———. 1999, in ASP Conf. Ser. 162, Quasars and Cosmology, ed. G. Ferland & J. A. Baldwin (San Francisco: ASP), 265
Green, P. J., Forster, K., & Kuraszkiewicz, J. 2001, ApJ, 556, 727
Green, P. J., et al. 1995, ApJ, 450, 51
Hamann, F., & Ferland, G. J. 1993, ApJ, 418, 11
———. 1999, ARA&A, 37, 487
Hamann, F., Korista, K. T., Ferland, G. J., Warner, C., & Baldwin, J. A. 2002, ApJ, 564, 592
Kaspi, S., et al. 1996, ApJ, 470, 336
Kaspi, S., Smith, P. S., Netzer, H., Maoz, D., Jannuzi, B. T., & Giveon, U. 2000, ApJ, 533, 631
Kauffmann, G., & Haehnelt, M. G. 2000, MNRAS, 311, 576
Kellermann, K. I., Sramek, R., Schmidt, M., Shaffer, D. B., & Green, R. 1989, AJ, 98, 1195
Kinney, A. L., Bohlin, R. C., Blades, J. C., & York, D. G. 1991, ApJS, 75, 645
Kinney, A. L., Rivolo, A. R., & Koratkar, A. P. 1990, ApJ, 357, 338
Korista, K. T., Baldwin, J. A., & Ferland, G. J. 1997, ApJS, 108, 401
———. 1998, ApJ, 507, 24
Korista, K. T., et al. 1995, ApJS, 97, 285
Lanzetta, K. M., Turnshek, D.,A., & Sandoval, J. 1993, ApJS, 84, 109
Laor, A., Bahcall, J. N., Jannuzi, B. T., Schneider, D. P., & Green, R. F. 1995, ApJS, 99, 1
Lawrence, A., & Elvis, M. 1982, ApJ, 256, 410
Malkan, M. A., & Sargent, W. L. W. 1982, ApJ, 254, 22
Mushotzky, R., & Ferland, G. J. 1984, ApJ, 278, 558
Netterfield, C., B., et al. 2002, ApJ, 571, 604
Netzer, H. 1985, MNRAS, 216, 63
———. 1987, MNRAS, 225, 55
Netzer, H., Laor, A., & Gondhalekar, P. M. 1992, MNRAS, 254, 15
Netzer, H., et al. 1995, ApJ, 448, 27
Osmer, P. S., Porter, A. C., & Green, R. F. 1994, ApJ, 436, 678
Osmer, P. S., & Shields, J. C. 1999, in ASP Conf. Ser. 162 Quasars and Cosmology, ed. G. Ferland & J. A. Baldwin (San Francisco: ASP), 235
Peterson, B. M., et al. 1993, ApJ, 402, 469
———. 1994, ApJ, 425, 622
Pettini, M. 1999, in Chemical Evolution from Zero to High Redshift, ed. J. Walsh & M. Rosa (Berlin: Springer), 233
Pogge, R. W., & Peterson, B. M. 1992, AJ, 103, 1084
Reichert, G. A., et al. 1994, ApJ, 425, 582
Santos-Lleó, M., et al. 2001, A&A, 369, 57
Sargent, W. L. W., Boksenberg, A., & Steidel, C. C. 1988, ApJS, 68, 539
Sargent, W. L. W., Steidel, C. C., & Boksenberg, A. 1989, ApJS, 69, 703
Schneider, D. P., Schmidt, M., & Gunn, J. E. 1991a, AJ, 101, 2004
———. 1991b, AJ, 102, 837
Schulz, H. 1992, in Physics of Active Galactic Nuclei, ed. W. J. Duschl & S. J. Wagner (Berlin: Springer), 235
Seaton, M. J. 1979, MNRAS, 187, 73
Shields, J. C., Ferland, G. J., & Peterson, B. M. 1995, ApJ, 441, 507
Steidel, C. C. 1990, ApJS, 74, 37
Steidel, C. C., & Sargent, W. L. W. 1991, ApJ, 382, 433
Stern, D., Djorgovski, S. G., Perley, R. A., de Carvalho, R. R., & Wall, J. V. 2000, AJ, 119, 1526
Stirpe, G. M., et al. 1994, ApJ, 425, 609
Storey, P. J., & Hummer, D. G. 1995, MNRAS, 272, 41
Storrie-Lombardi, L. J., McMahon, R. G., Irwin, M. J., & Hazard, C. 1996, ApJ, 468, 121
Tananbaum, H., Avni, Y., Green, R. F., Schmidt, M., & Zamorani, G. 1986, ApJ, 305, 57
Telfer, R. C., Zheng, W., Kriss, G. A., & Davidsen, A. F. 2002, ApJ, 565, 773
Turnshek, D. A. 1997, in ASP Conf. Ser. 128, Mass Ejection from Active Galactic Nuclei, ed. N. Arav, I. Shlosman, & R. J. Weymann (San Francisco: ASP), 52
Vanden Berk, D. E., et al. 2001, AJ, 122, 549
Véron-Cetty, M.-P., & Véron, P. 2001, A&A, 374, 92
Véron-Cetty, M.-P., Véron, P., & Tarenghi, M. 1983, A&A, 119, 69
Vestergaard, M., & Wilkes, B. J. 2001, ApJS, 134, 1
Wampler, E. J., Gaskell, C. M., Burke, W. L., & Baldwin, J. A. 1984, ApJ, 276, 403
Wandel, A. 1999a, ApJ, 527, 649
———. 1999b, ApJ, 527, 657
Wanders, I., et al. 1997, ApJS, 113, 69
Wang, T.-G., Lu, Y.-J., & Zhou, Y.-Y. 1998, ApJ, 493, 1
Weymann, R. J., Morris, S. L., Foltz, C. B., & Hewett, P. C. 1991, ApJ, 373, 23
Weymann, R. J., et al. 1998, ApJ, 506, 1
Wilkes, B. J., Kuraszkiewicz, J., Green, P. J., Mathur, S., & McDowell, J. C. 1999, ApJ, 513, 76
Wilkes, B. J., Tananbaum, H., Worrall, D. M., Avni, Y., Oey, M. S., & Flangan, J. 1994, ApJS, 92, 53
Wills, B. J., Laor, A., Brotherton, M. S., Wills, D., Wilkes, B. J., Ferland, G. J., & Shang, Z. 1999, ApJ, 515, L53
Wills, B. J., et al. 1995, ApJ, 447, 139
Zamorani, G., Marano, B., Mignoli, M., Zitelli, V., & Boyle, B. J. 1992, MNRAS, 256, 238
Zheng, W., Fang, L.-Z., & Binette, L. 1992, ApJ, 392, 74
Zheng, W., Kriss, G. A., & Davidsen, A. F. 1995, ApJ, 440, 606
Zheng, W., Kriss, G. A., Telfer, R. C., Grimes, J. P., & Davidsen, A. F. 1997, ApJ, 475, 469
Zheng, W., & Malkan, M. A. 1993, ApJ, 415, 517